A Modular Framework for Performance-Based Durability Engineering: from Exposure to Impacts

Madeleine M. Flint[a,*], Jack W. Baker[a], Sarah L. Billington[a]

[a] *Stanford University, Department of Civil and Environmental Engineering, Stanford, CA, USA*

Abstract

A modular framework for assessing the economic, environmental, and social impacts of structural durability has been proposed and applied to a concrete structure expected to undergo climate-change-accelerated chloride-induced reinforcement corrosion. The proposed performance-based durability engineering (PBDE) framework comprehensively considers uncertainty, accommodates non-stationary exposure, and computes quantitative sustainability metrics. Drawing on previous work in the nuclear risk and earthquake engineering communities, PBDE's three analysis stages are de-coupled at pinch-points, allowing the use of a convolution integral to link uncertainty in exposure, deterioration and repair, and sustainability impacts. The convolution-based methodology for the PBDE framework has been compared with traditional Monte Carlo simulation. Results of the convolution approach were statistically equivalent to brute-force Monte Carlo analysis using the same number of simulations, and the convolution approach has advantages in deaggregation, backwards conditioning, and updating of results to reflect new information or models. Limitations of the convolution approach are discussed, as are possible techniques for decreasing computational expense and areas for future work. Potential applications for PBDE include design code calibration, decision support for climate change adaptation policy, and sensitivity assessment to direct research.

Keywords:
durability, sustainability, performance-based engineering

1. Introduction

The design and renewal of sustainable and resilient infrastructure pose challenges to managers operating under funding constraints and changing use and exposure conditions. Numerous studies note a backlog of infrastructure renewal in the United States; reducing this backlog demands efficient allocation

*Corresponding author
Email addresses: flint@stanford.edu (Madeleine M. Flint), bakerjw@stanford.edu (Jack W. Baker), billington@stanford.edu (Sarah L. Billington)

of resources to address the most critical structures [1]. In the US transportation sector, the cost of rehabilitating approximately 67,000 structurally deficient bridges is estimated at $33 billion USD [2]. Approximately 80% of all US bridges and 50% of structurally deficient bridges were constructed prior to 1960, which suggests likely growth of the current backlog without implementation of a substantial preventive maintenance program.

The need for additional infrastructure renewal to adapt to the changing climate will further stretch resources, and will require balancing costs, environmental impacts, and societal risk. Climate change is predicted to increase the rate of damage caused by corrosion of black steel reinforcement in concrete structures [3–6], the most common cause of reinforced concrete deterioration [7]. In the US, over 65% of all bridges and 34% of structurally deficient bridges have reinforced or prestressed concrete substructures and superstructures; many other bridges have reinforced concrete decks [2]. Cement and steel production in the US were estimated to emit 96.5 million metric tons of greenhouse gases (CO_2 eq.) in 2011 [8], and cement production comprises approximately 5% of annual worldwide anthropogenic carbon dioxide emissions [9]. The high environmental impacts of infrastructure materials create a self-reinforcing cycle: unsustainable infrastructure design worsens climate change, thereby reducing infrastructure durability, resiliency, and sustainability, and spurring further, unsustainable, infrastructure renewal. To support rational infrastructure management, federal, state, and municipal agencies in the United States have demanded quantitative performance metrics for sustainability [10]. Decision-makers must aim to ensure a low and acceptable degree of natural hazards risk while meeting sustainability goals, which in turn requires consideration of uncertainty in efforts to curb emissions, climate sensitivity, and the impact of climate change on structural durability and performance.

Due to the importance of providing decision support for infrastructure design, management, and rehabilitation, many approaches to durability design have recently been proposed or refined, e.g., [4; 6; 11–17] for reinforced concrete structures. Existing durability design approaches balance merits and constraints; lack of applicability to multiple types of infrastructure, inability to select from a variety of models, and inadequate consideration of climate change are common limitations. Several approaches currently employed by transportation infrastructure managers may not accurately predict deterioration in changing use and exposure conditions. These methods are also in many cases insufficient to assess innovative designs or repair strategies. While researchers have addressed some limitations, many existing research approaches do not extend to the fully-probabilistic economic, social, and environmental decision support data required by operators. A more general and flexible methodology is needed to tie together research models in a decision-oriented approach.

A framework is proposed herein to circumvent common limitations and to provide a comprehensive methodology for structural durability assessment. Drawing on related methodologies used in probabilistic risk assessment for earthquake engineering, a performance-based approach is taken [18–20]. Performance-based approaches emphasize the direct computation of engineering variables of

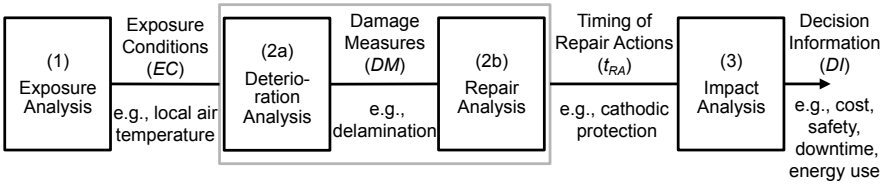

Figure 1: Stages and pinch-points of the PBDE assessment. Simulations are performed in stages based on a limited number of pinch-point variables passed on from the preceding analysis stage.

interest through the use of mathematical models, rather than the use of prescriptive approaches intended to ensure acceptable performance. The proposed framework considers uncertainty in all analysis stages, similar to many risk frameworks in other application domains, yet distinctly new relative to the majority of durability frameworks.

As first proposed in [21], the framework offers conceptual clarity in assessing infrastructure performance by separating the contributions of multiple disciplines into discrete analysis stages. Robust decision support is provided by combining the uncertainty associated with each analysis stage. The framework links a series of conditionally independent analysis stages at "pinch-points," where only a few variables are passed from one stage to the next, as shown in Fig. 1. Stage (1), exposure analysis, links assumptions about future emissions and weather patterns to simulations of exposure conditions, such as air temperature and precipitation, at the site. Deterioration analysis, stage (2a), uses exposure condition time series to predict the evolution of detectable damage measures, such as the presence of cracking, over time. These damage measures are passed to repair analysis, stage (2b), for simulated inspections to determine whether or not a repair action, such as cathodic protection or surface treatment, is applied. Finally, in stage (3), impact analysis, an inventory of the costs, downtime, and environmental impacts of the different repair actions is used to calculate decision data for combinations of repair timing.

The proposed framework can be applied to different structures and exposures, and its modularity allows models to be interchanged within each analysis stage with minimal effect on other stages. The comprehensive inclusion of uncertainty from exposure to final decision data can lead to the accumulation of large uncertainties in output decision information. However, this uncertainty can be traced back to its origin through deaggregation and backwards conditioning, and the approach accurately accounts for the randomness inherent to infrastructure performance. PBDE may be preferred to other approaches when it is desirable to trace the influence of several sources of uncertainty, to compare the predictions of multiple climate or deterioration models, or to develop fully-probabilistic descriptions of multi-attribute decision data.

This paper discusses the background of the proposed PBDE framework and other durability engineering approaches. Descriptions of the methodology and each analysis stage are followed by an example to illustrate application of the

framework. Results obtained using the proposed convolution-based methodology for the PBDE framework are compared to results using a traditional Monte Carlo approach. Finally, conclusions regarding the usefulness of the methodology, anticipated limitations, and future work are discussed.

2. Background

The proposed framework relates to a broad context of research, including reliability and risk theory, and decision-support methods. Previous applications of performance-based design to durability have focused on service life as a proxy for performance, e.g., [14; 17], or the optimization of more direct performance metrics such as costs [15]. The proposed framework is analogous to other methodologies developed for performance-based engineering and design, especially those targeting nuclear risk and earthquake engineering.

2.1. Durability engineering methodologies

Durability engineering methodologies share the goal of improving decisions made in the design of new structures and repair of existing structures, but differ widely along three measures. The approaches are split between those that compute direct decision-making information such as cost, and others that consider implicit metrics such as service life. Approaches from both implicit and explicit decision orientations use physics-based, empirical, or survey-derived deterioration models. Some approaches incorporate uncertainty whereas others are deterministic. Background on various approaches is given in the following sections according to the major distinction between service life prediction and optimization of decision-making information.

2.1.1. Service life prediction

Service life prediction methodologies attempt to ensure acceptable structural durability by calculating expected service life for different geometries, materials, and inspection and maintenance strategies. Methods of modeling deterioration and service life range from empirical models derived from surveyed condition data to coupled, physics-based, numerical models. Practitioner-oriented guides to design and rehabilitation tend to use analytical models, but vary from limited inclusion of uncertainty, e.g., [16; 22], to full consideration, e.g., [17]. Load and resistance factor design (LRFD) [11], a variety of reliability methods, including first order reliability method (FORM) [23], Monte Carlo assessment [6], and fuzzy set theory [14], among many others, have recently been proposed as durability design frameworks. These approaches may focus on adequate material design [14], or at a combination of material, geometry, and efforts to limit exposure [24]. Some approaches consider climate change scenarios, e.g., [3–6], or structural safety, e.g., [6; 23], which are also included within the scope of the proposed PBDE framework.

Approaches within service life prediction vary in strengths and limitations. Using service life as a proxy for performance is stable: decision results are not

dependent on cost fluctuations or discount rates. Approaches pairing simple deterioration modeling with deterministic assessment are easy to implement and provide preliminary design guidance. Advanced models are capable of simulating service life under a wide variety of exposures, and can be used to assess innovative materials and repair actions. However, simple models may be inaccurate compared to more sophisticated models, whereas advanced models require a greater number of parameters that may not be readily available.

2.1.2. Maintenance and repair optimization

Maintenance and repair optimization approaches focus on decision information such as costs, environmental impacts, and safety, or utility functions of this information. Many recent approaches propose methods for optimizing design and maintenance of reinforced concrete infrastructure, including through use of Markov chains [12], Bayesian nets [13], renewal theory [25] and cellular automata [26], among others. These approaches frequently utilize probabilistic descriptions of deterioration derived from surveys of existing structures, and may require large datasets to produce robust predictions. Discrete Markov chains, which link a damage state at one time step to the probability of moving into a more severe damage state at the next time step, are commonly used in bridge management system software [27]. A hybrid approach has been proposed in [28] that combines the physics-based modeling of deterioration commonly used in service life prediction with a Markovian approach more suited to maintenance optimization.

Like service life prediction approaches, maintenance and repair optimization methods balance strengths and limitations. In general, these optimization approaches are practical: they focus on the development of decision information needed to select maintenance and repair strategies, and can be used to model a variety of structural elements. However, deterioration models derived from survey data may not be robust when data is limited, or when new climates or materials are studied. While hybrid approaches, e.g., [28], are in theory capable of optimizing maintenance in a changing climate, few studies consider both climate and impact uncertainty as proposed in PBDE. Furthermore, in some cases the focus on decision optimization leads to scarce availability of intermediate information for validation of deterioration predictions. Given the difficulty of managing large infrastructure networks, maintenance and repair optimization methods offer valuable insight into possibilities for improving network-level performance.

2.2. Performance-based risk engineering methodologies

Performance-based methods directly evaluate life-cycle outcomes by predicting and quantifying the range of behavior of engineered systems. Many probabilistic risk assessment methodologies compute decision-making information by combining conditionally independent analyses. Nuclear risk engineering methodologies, e.g., [18], generally separate an assessment into several analysis stages, incorporate uncertainty in each stage, and propagate uncertainty to obtain descriptions of decision variables. These techniques were further developed

in performance-based earthquake engineering (PBEE), where they have been used to update building codes, design special structures, and to conduct large scale studies for use in policy [19; 20]. Performance-based methodologies for earthquake developed by the Pacific Earthquake Engineering Research Center (PEER) [19] have been adapted to wind [29] and other natural hazards, and are closely related to the PBDE framework proposed herein. These performance-based frameworks are significant for their usefulness in guiding code design and policy, and for their identification of future research needs. In applying PEER performance-based approaches to climate-influenced natural hazards, care must be taken to assure that the assumptions used to develop a hazard curve are consistent with non-stationary extreme event risk; the proposed PBDE framework supports consideration of non-stationary hazards. Other recent work has linked performance-based assessment of sustainability and natural hazard risk, including assessment of repair practices [30]. While performance-based probabilistic risk assessment is but one of many methods for managing risk [31], it has been widely and successfully used in civil engineering.

3. Proposed probabilistic framework

The proposed methodology for performance-based durability engineering analyzes a given structure and site in three stages: (1) exposure, (2a) deterioration and (2b) repair, and (3) impact. The results of these stages are sets of generalized "pinch-point" variables: exposure conditions (EC), damage measures (DM), repair action timing (t_{RA}), and decision information (DI), respectively. Deterioration and repair analysis occur in the same stage due to the dependency of deterioration on previous repair actions. All analysis stages may give rise to large uncertainties, both aleatory and epistemic, which are incorporated into the full probabilistic assessment.

Each analysis stage computes a complementary cumulative distribution, denoted G, of the probability of exceeding a value of the considered pinch-point variable. For deterioration, repair, and impact analyses, these distributions are conditioned on a given value of the pinch-point variable output from the prior analysis stage. Convolving a series of these conditional distributions using Eq. 1 yields a final distribution for lifetime decision information.

$$G_{DI}(di) = \iint G_{DI|t_{RA}}(di|t_{ra}) \left|dG_{t_{RA}|EC}(t_{ra}|ec)\right| \left|dG_{EC}(ec)\right| \tag{1}$$

The incorporation of initial construction decision information, e.g., in order to compare alternative new designs that vary in up-front and long-term expected costs, is possible through an additional convolution integral or through Monte Carlo simulation. Use of the convolution integral assumes that initial decision information distributions are independent of repair-related decision information, as in Eq. 2, where f denotes a probability density function (PDF). If the distributions are not independent, Monte Carlo sampling of the initial construction and repair-related decision information distributions allows computation of the full lifetime distribution.

$$G_{DI}(di) = \int G_{DI,t>0}(di - z) f_{DI,t=0}(z)\, dz \tag{2}$$

The following descriptions of the analysis setup and stages refer primarily to models required for predicting chloride-induced corrosion in coastal reinforced concrete bridges, though the methodology is not limited to this case. Provided that appropriate deterioration models are available, other structures and mechanisms may be studied, including wood rot in residential housing, façade damage of historic buildings, corrosion of steel infrastructure, or any other mechanism in which damage accumulates over time.

3.1. Analysis setup

PBDE assessments require many parameters and assumptions, including: structural geometry, material properties, weather data, deterioration mechanisms likely to affect the structure, and inspection and repair practices. Key decisions in analysis setup include the selection of appropriate deterioration mechanisms and related models, and the determination of the scope of uncertainty to be included. Treating model parameters, material properties, and structural geometry as random variables may greatly increase the number of simulations required in deterioration and repair analysis. Preliminary studies conducted during analysis setup determine an appropriate discretization of the pinch-point variables and the number of simulations required in each analysis stage.

3.2. Exposure analysis

Exposure analysis simulates local weather exposure conditions (ECs) at the studied site. In addition to meteorological data, other causes of deterioration, including applied loads, can also be modeled, e.g., to study the interaction of load-induced cracking and transport of aggressive ions. The models used in exposure analysis may take both global-scale inputs, e.g., greenhouse gas emission scenarios, and local-scale inputs, e.g., ground surface roughness near the site. The most sophisticated analyses would include emissions models, a global climate model ensemble, a regional climate model, and models that translate local weather conditions to exposure conditions acting on the structural surface, e.g., wind-driven rain models. The outputs from the exposure models include both "records" (time series) of exposure to be used in deterioration analysis, and a probabilistic distribution of the likelihood of experiencing a record consistent with a characteristic level of severity, i.e., a characteristic exposure distribution (G_{EC}). Fig. 2 illustrates components of a characteristic exposure condition: baseline mean annual temperature, described by a generic variable, $\hat{\lambda}$, and annual temperature "noise" and trend terms. The three terms are summed to compute the characteristic exposure condition, increase in mean annual temperature over the lifetime. A distribution of the characteristic exposure condition can be obtained by weighting different emissions scenarios, e.g., from [32], or by fitting a distribution to the output of a climate model.

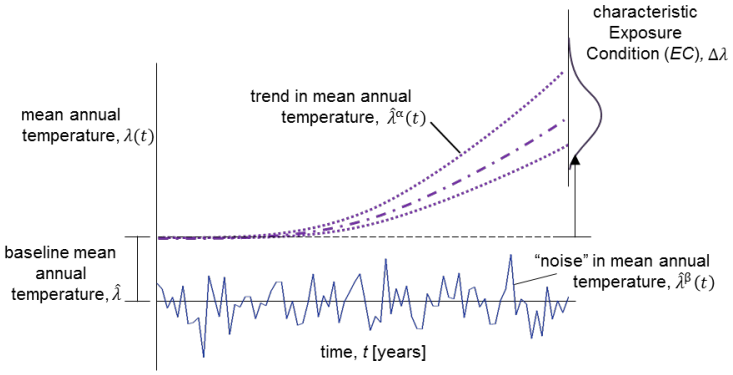

Figure 2: Representation of example exposure analysis with characteristic distribution of increase in mean annual temperature and exposure "record" components.

Selection of an efficient and sufficient characteristic condition can present difficulties. The characteristic exposure condition must allow for simulation of other exposure condition records consistent with a sampled value. If, for example, the selected characteristic condition is increase in mean annual global temperature, records of local temperature, humidity, precipitation, etc., should be simulated based on assumptions consistent with the sampled value of the mean temperature increase. Due to the large variability in local weather, it is likely that a suite of exposure condition records consistent with a single value of the characteristic EC is needed to capture exposure uncertainty. An efficient characteristic exposure condition minimizes damage and repair variability at a given level of exposure, thereby limiting the number of computationally-expensive deterioration/repair simulations. Substantial research in the PBEE community has studied methods for the selection of that framework's analogous pinch-point hazard variable, and has proposed several alternative candidates [33].

3.3. Deterioration analysis

Deterioration analysis relates exposure at the site to observable or detectable structural damage. Records of exposure conditions are passed to one or more empirical or physical deterioration models to simulate the accumulation of material and component degradation. Degradation is linked to damage measures selected from common visual or special inspection methods, which act as indicators, or thresholds, to trigger repair actions in the concurrent repair analysis stage. Deterioration analysis outputs simulations of damage measures, and conditional distributions of the probability of exceeding damage over time ($G_{DM|EC}(dm, t|ec)$). These distributions are not included in the calculation of decision information, but are used in safety and reliability assessments, and are generally of interest to maintenance engineers.

Several challenges are present in deterioration modeling, including spatial correlation and multi-mechanism issues discussed in Sec. 3.6, and other issues

surrounding model selection and the simulation of boundary conditions. In reality, deterioration mechanisms may be tightly coupled, and few physical models capture the interdependent nature of structural deterioration. Furthermore, physics-based transport models require methods to compute nonlinear heat, moisture, and ion surface boundary conditions. Considerable research within the building physics community has focused on the development of methods to compute heat and moisture surface conditions [34], which have not been widely implemented in infrastructure durability research [6]. Sensitivity of infrastructure deterioration to boundary conditions depends on the sophistication of heat and mass transport and damage models used, which range in complexity and degree of coupling. In the modeling of corrosion damage in reinforced concrete, this range extends from use of apparent Fickian diffusion for chloride transport [24], to numerical models that fully couple heat and mass transport with corrosion, e.g., [35]. An intermediate de-coupled numerical approach was used to develop the illustration presented in Sec. 4. In addition to the differing requirements for exposure data resolution, model selection typically involves tradeoffs between accuracy, computational expense, ease-of-use, and availability of required material parameters. Discrepancies in predictions of deterioration rates and sensitivity to boundary conditions between different types of heat and mass transport models have been found in [36]; the proposed PBDE framework offers a means to assess the importance of these discrepancies through comparison of decision outcomes.

3.4. Repair analysis

Repair analysis captures the decision-making process of operators in order to determine when and how a damaged structure or element is repaired. In addition to the damage measure simulations, inputs to repair analysis include the proposed inspection timing and practices, a set of possible repair actions, and information on conditions that will lead to the selection of a particular repair action. In the method of repair analysis currently used, the input information is mapped onto a decision tree relating damage measures observed during an inspection event to the selection of a repair action. The decision tree used in the illustration example, that of a coastal reinforced concrete structure, is shown in Fig. 3. While records of repair events are available from repair analysis, the primary output from this stage is the conditional repair action timing distribution ($G_{t_{RA}|EC}(t_{ra}|ec)$) calculated from the discrete probabilities of observing a particular combination of individual repairs, given a value of the characteristic exposure condition. For example, given two possible repair actions, a repair timing combination, K, might be denoted $t_{RA_K} = \{\ t_{ra_1} = 10$ years; $t_{ra_2} = 30$ years$\}$.

Several factors may complicate the development of a rational and computationally efficient decision tree, including the use of life-cycle costing or structural analysis within the decision tree, operators who do not have set repair practices, and lack of data or guidelines on what values of damage measures trigger repair. When the repair actions or damage thresholds are unclear, reviewing past inspection and repair records may be helpful. In any case, engineering judgment

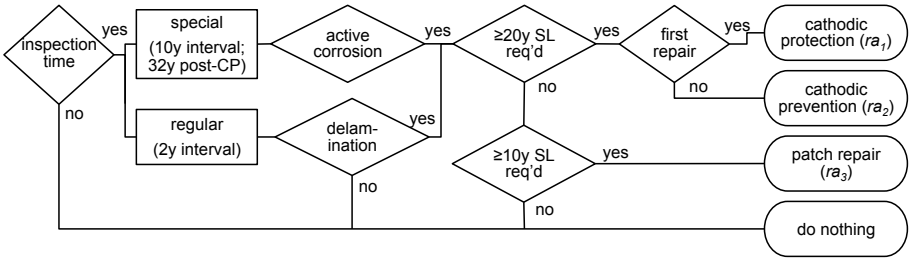

Figure 3: Decision tree for repair actions (RA) cathodic protection (CP), cathodic prevention after end of CP system functionality, and patch repair. Special and regular inspections occur at ten and two-year intervals, respectively. Decisions to repair are based on the damage measures (DM) presence of delamination and finding of an active corrosion state, as well as the current repair state and required remaining service life (SL).

is required to develop even a "best practices" tree, which leads to a possible discrepancy between PBDE assessment results and actual outcomes. However, if a rational management practice is planned, PBDE assessment allows comparison of alternative strategies or designs.

3.5. Impact analysis

Impact analysis links a combination of repair action timing to the economic, environmental, and social impacts of the repairs. Economic decision information includes both direct measures, such as the cost of repairs, and indirect measures, such as economic loss due to building closure or traffic delays. Direct costs can be obtained through process-based costing [37], where a cost is obtained for each material or construction action, or through cost estimates for the entire repair action, i.e., from bid data. Environmental impacts include emission of greenhouse gases and other air pollutants, energy use, release of toxic chemicals, and several additional midpoint indicators. In many cases an inventory of materials, equipment, and energy used in repair is required for cost and environmental impact modeling. Indirect costs and social impacts related to structural safety require additional data on use patterns. The output from impact analysis is a set of conditional distributions for decision information given repair action timing ($G_{DI|t_{RA}}(di|t_{ra})$). If many repair actions timing combinations and decision information variables are considered, the number of conditional distributions may become large, in which case only those conditional distributions reflecting active combinations of repairs might be computed.

Significant sources of uncertainty are present in the calculation of repair impacts, including: uncertainty in which construction methods contractors will select; uncertainty in quantities of materials used; variation in material resource allocation and processing worldwide; uncertainty in the future economy, including discounting and inflation; uncertainty in the future energy mix and other technological developments; and uncertain future populations, structure use, and occupancy. For environmental impact assessment, selection of a method involves tradeoffs between sources of uncertainty: environmental input-output (EIO)

models capture the coupled and nested intricacies of environmental impacts but cannot distinguish between local-level variations, whereas process-based life cycle assessment can capture local practices but requires inventory data that may not be readily available. Hybrid approaches combine the comprehensive aspects of economic input-output modeling with the specificity of process-based approaches, and are commonly used in practice. Cass and Mukherjee [38] discuss the benefits and drawbacks of the various approaches as applied to pavements. Several recent bridge life cycle assessments have been reviewed in [39], which compares six environmental indicators for three real bridges of varying material and structural form.

In addition to their uncertainty, the some impacts are likely to be correlated, e.g., an individual repair action might be more difficult to perform than average, resulting in both high costs and high closure time. PBDE assessment can determine the effect of partial correlation. Given the numerous and potentially large sources of uncertainty, the analyst may prefer to take a first-order approach by assigning independent normal distributions for all initial and ongoing impacts, allowing direct calculation of (normal) impact distributions for sets of repair action timing. This first-order method was used in the illustration presented in Section 4. With some modification, this approach could be used to assess the sensitivity of results to assumptions of future costs or technology.

3.6. Challenges and mitigation approaches

The breadth of the proposed framework leads to large computational and data intensity, which must be mitigated to effectively perform PBDE assessment. Models used within exposure and deterioration analysis stages may be individually computationally intensive, and their combination in PBDE may lead to lengthy analysis times for a single simulation. Adding to the complexity is the need to predict exposure and deterioration in multiple, disparate parts of the structure: repair analysis considers repair actions that may be selected based on the state of the entire structure, rather than the state of one portion of one component. This need to consider system states requires additional effort to select appropriate deterioration mechanisms for each component, again increasing computational expense. To make the PBDE assessment more tractable, the analyst might use spatial correlation models to simulate random fields [40–42], sampling techniques [43], or other methods drawn from related performance-based methodologies.

Furthermore, in-situ exposure rarely matches the assumptions used to develop common single-mechanism deterioration models. Interaction of multiple deterioration mechanisms frequently accelerates overall deterioration; performing separate PBDE assessments for different types of damage and adding the results is not possible. When it is important to capture multiple deterioration mechanisms, general deterioration approaches, e.g., the use of Markov transition matrices, may be implemented within the PBDE assessment. The Markovian approach will yield the most realistic results when the studied structure closely matches conditions used to derive the transition matrices, i.e., for common structure materials, types, and load patterns, and when climatic conditions

are expected to remain stable. In no case will a PBDE assessment completely describe all possible scenarios and impacts, but baseline results can allow for comparison of alternative designs or repair strategies.

4. Demonstration of methodology and comparison to a Monte Carlo approach

An idealized reinforced concrete coastal structure was selected to demonstrate the use of the proposed PBDE methodology and to compare the convolution method with traditional, "brute force" Monte Carlo simulation. Simplifying assumptions increased the clarity of the illustration and minimized the computational expense associated with performing both convolution and Monte Carlo assessments. Section 6.4 identifies possible extensions to more sophisticated assumptions or models. Results included predictions of the course of damage over time and final cost and downtime impact distributions. An additional study used the convolution approach to analyze contributions to decision information uncertainty, and to update decision information distributions to reflect a change in the exposure emissions scenario.

4.1. Structure, site, and deterioration mechanism

An idealized reinforced concrete coastal structure was studied for risk of chloride-induced reinforcement corrosion. The structure was assumed to be constructed in 2010 with planned demolition in 2090, necessitating inclusion of potential climate change in exposure analysis. The illustration considers high and low emissions scenarios combined with global climate uncertainty. The chosen site of coastal Hilo, Hawaii, and functional unit of a sheltered, vertical surface, allowed use of ambient meteorological data as surface boundary conditions with minimal error compared to splash zone or tidal exposure. The moderate temperature and humidity range of Hawaii causes a high degree of corrosion risk while reducing the potential for multi-mechanism deterioration. A standard ordinary Portland cement concrete mix design with water-to-cement ratio of 0.5 and cover depth of 50 mm was studied over a functional unit of a 1 m^2 surface area. The selection of a planar element minimized localization and edge effects, allowing the use of one-dimensional transport models.

4.2. Models used in analysis stages

4.2.1. Exposure analysis models

Increase in the mean annual temperature at year 2090 over the 1970 baseline served as the characteristic exposure condition. The temperature projections used in this study were based on a report on climate change in the South Pacific islands, which accounted for a set of emissions scenarios representing divergent technology development and adaptation, economic and population growth, and favored fuel type [32; 44]. In addition to increased mean temperature and sea level rise, climate change is expected to induce more frequent downpour and

extreme high sea level events in this region. Based on "high" and "low" emissions scenarios and climate projections, possible warming in this region ranges from 1.4 to 3.4℃ by year 2090, relative to a 1970 baseline. Increase in mean annual temperature at 2090 was modeled as the sum of equally-weighted normal random variables representing "high" and "low" emissions scenarios, according to Eq. 3, where $\mathcal{N}$ denotes a normal distribution. A power law was assumed for the functional form of the climate projections in [44]; parameters for the power law representation of temperature increase (λ^{α}) were modeled as functions of the characteristic exposure condition and obtained through regression. The convolution assessment discretized the exposure condition over the range 1.1 to 3.5℃.

$$\begin{aligned} EC &\sim 0.5\mathcal{N}(1.80, 0.20) + 0.5\mathcal{N}(3.00, 0.13) \\ \lambda^{\alpha}(t_{year}) &= a_{ec}(t_{year})^{n_{ec}} \\ a_{ec}(ec) &= 5.04\text{E-}3ec^2 - 3.57\text{E-}2ec + 6.49\text{E-}2 \\ n_{ec}(ec) &= 3.59\text{E-}1ec + 3.33\text{E-}1 \end{aligned} \tag{3}$$

The characteristic exposure condition was combined with other parameters and assumptions to develop temperature, relative humidity, and chloride concentration surface boundary condition records representative of atmospheric coastal exposure. All surface boundary condition records were computed using Eq. 4 and parameters from Table 1, where the generic variable λ represents any of the three types of exposure conditions. For temperature, T, local climate parameters were calculated from 1970-2012 data recorded at Hilo International Airport, Station ID CCOP:511492, obtained from the NOAA NCDC database (`http://www.ncdc.noaa.gov/`). A term (λ^{β}) reflecting natural year-to-year variation in Hilo's climate was modeled as a set of zero-mean "noise" (ϵ) with standard deviation of 0.475℃, and added to Hilo's baseline average mean annual temperature ($\hat{\lambda}$). The convolution assessment used the same set of independent noise records at each value of characteristic exposure, whereas the Monte Carlo assessment used a unique, independent noise record for each individual simulation. In order to characterize seasonal temperature variation (λ^{s}), a harmonic term was added based on regression performed on the meteorological data. Seasonal variations are not expected to change significantly under rising mean annual temperature in this region [44]. The approach taken herein of adding independent terms to reflect global and local climate behavior simplifies the complex interaction between climate spatial scales.

$$\begin{aligned} \lambda(t) &= \hat{\lambda} + \lambda^{\alpha}(t_{year}) + \lambda^{\beta}(t_{year}) + \lambda^{s}(t) \\ &= \hat{\lambda} + a_{ec}(t_{year})^{n_{ec}} + \epsilon(t_{year}) \\ &+ a_1 \sin(\omega t + b_1) + a_2 \sin(2\omega t + b_2) \end{aligned} \tag{4}$$

Annual mean relative humidity, h, and annual mean exposure to surface chlorides, C_{Cl}, were assumed constant both year-to-year and with increasing

Table 1: Parameters for exposure boundary condition equations

λ	$\hat{\lambda}$	λ^{α}	λ^{β}	λ^{s}			
		ec	ϵ	a_1	b_1	a_2	b_2
T [°C]	23.3	1.1–3.5	$\sim\mathcal{N}(0,0.475)$	1.46	2.64	0	0
h [-]	0.735	0	-	9.49E-3	-0.813	0	0
C_{Cl} [%kg/kg cem]	84.6	0	-	57.2	1.24	16.5	0.172

temperature. Relative humidity seasonal variation was based on a regression on ambient meteorological data. Surface chloride concentration seasonal variation was based on a combination of survey data and a study of seasonal variation in marine aerosol salinity, details of which can found in [36]. The annual mean surface concentration was of similar magnitude to the "high" exposure in [6] and the "atmospheric coastal" exposure in [4].

4.2.2. Deterioration analysis models

Deterioration analysis modeled chloride transport, reinforcement corrosion initiation, corrosion propagation, and concrete cover delamination, as shown in Fig. 4. Use of a temperature- and moisture-dependent Fickian diffusion partial differential equation was amenable to the level of sophistication of exposure modeling. The diffusion equation was solved numerically, rendering it capable of predicting transport under non-stationary boundary conditions and preventing errors associated with commonly-used analytical approximations [45]. The empirical, stochastic corrosion propagation model is a function of temperature and chloride concentration. With the exception of corrosion initiation and delamination critical values, the model parameters were deterministic. While the Monte Carlo assessment sampled stochastic parameters directly from their distributions, the convolution assessment used an optimized uniform Latin hypercube scheme. Uniform Latin hypercube offers improved sampling efficiency over brute-force Monte Carlo in building envelope hygrothermal modeling [43]. The routine to determine an optimal uniform sampling scheme provided in [43] is an adaptation of the "maximin" optimization algorithm in [46]. A more detailed description of the deterioration modeling and required parameters is presented in Appendix A.

4.2.3. Repair analysis models

Inspection was assumed to occur at two-year intervals from 2012 to 2080. At "regular" inspections repair analysis simulated inspection of the surface for delamination. Every ten years (2020, 2030, ...) nondestructive evaluation of corrosion rates was simulated. Three repair options were considered: cathodic protection, ra_1, followed by cathodic prevention, ra_2, if the remaining service life was greater than or equal to 20 years, or by patch repair, ra_3, when from 10 to 20 years of service were required. Titanium anode mesh cathodic protection, including removal of the concrete cover and application of repair mortar, was assumed functional for 30 years, with 2 years of remaining protection after the end of system life [22; 47]. If indicated, installation of cathodic prevention

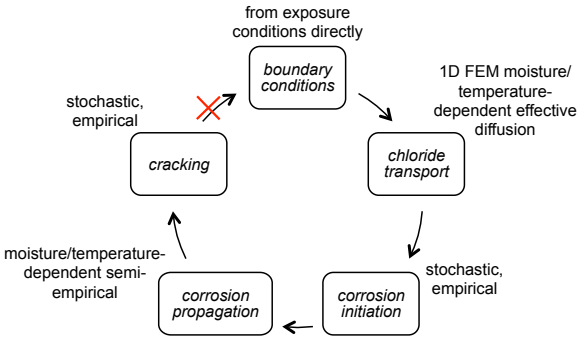

Figure 4: Schematic of deterioration models used in the demonstration.

Table 2: Impact inventory for repair actions assuming a functional unit of a 1 m^2 vertical reinforced concrete surface area

Repair Action	Initial Cost [USD]	Ongoing Cost [USD/yr]	Downtime [months]
Cathodic protection	$\sim \mathcal{N}(250, 80)$	$\sim \mathcal{N}(5, 1)$	$\sim \mathcal{N}(24, 6)$
Cathodic prevention	$\sim \mathcal{N}(150, 40)$	$\sim \mathcal{N}(5, 1)$	$\sim \mathcal{N}(6, 2)$
Patch repair	$\sim \mathcal{N}(100, 20)$	-	$\sim \mathcal{N}(4, 1)$

after the failure of the cathodic protection system was assumed to maintain sufficient polarization of the reinforcement to prevent active corrosion initiation. The cathodic prevention system was also assumed effective for 32 years. Patch repairs using mortar were assumed to occur over one-quarter of the functional unit (0.25 m^2). It was assumed that no repair would occur after failure of the patch repair or cathodic prevention system, or with less than 10 years remaining service. The repair tree yielded 51 possible combinations of repair action timing.

4.2.4. Impact analysis models

The assessment focused on two types of readily-characterized decision information: cost and downtime for repair. Cost and downtime were modeled using estimates from [22; 47; 48]. For the assessment herein, downtime was considered disruption of normal activity rather than complete loss of use, resulting in relatively long possible downtimes. All decision information was modeled as normally distributed, with means and standard deviations given in Table 2. Cost and downtime were assumed stationary and uncorrelated. This assumption allowed direct calculation of the parameters of normally-distributed decision information from the parameters of the individual repair impacts.

4.3. Numerical implementation

The PBDE assessment was carried out in a series of Matlab 2012b scripts. The range and discretization of time, damage measures, and decision information was determined through convergence studies. The final scheme for convo-

lution resulted in discretization of 10 exposure condition values and 100 deterioration/repair simulations per exposure condition value. The same number of total simulations (1000) was used for both convolution and Monte Carlo approaches, although more thorough investigation might have reduced the number of simulations in either case.

Histograms were used as conditional and final damage measure distributions. Empirical complementary cumulative distributions were used for all Monte Carlo approach distributions; the decision information means and standard deviations were obtained directly from the simulated values. Numerical convolution of the conditional distributions according to Eq. 1 used a trapezoidal integration rule. The Kolmogorov-Smirnov (K-S) test, which allows statistical testing of non-parametric distribution, was used to compare the convolution and Monte Carlo results, using the one-sample or two-sample test as appropriate. Reported p-values give the probability of observing a value of the maximum difference (supremum) between two cumulative distribution functions (CDFs) based on the hypothesis that the distributions are equivalent.

5. Results

5.1. Final results

5.1.1. Exposure analysis results

Exposure analysis results reflected the primary assumption of a combination of normal distributions for the characteristic exposure condition, increase in mean annual temperature. Exposure analysis discretized the range of the characteristic exposure condition into 10 values; the resulting distribution is shown in Fig. 5, along with the empirical distribution obtained from the Monte Carlo samples, and the original distribution. By the one-sample K-S test, the Monte Carlo empirical CDF was consistent with the specified distribution, which confirmed that a sufficient number of simulations were performed for this variable (p=0.98).

5.1.2. Deterioration analysis results

Temporal evolution of the probability density function for chloride concentration at 50 mm is shown in Fig. 6. The contour plot was derived from the convolved data, which branched into eight behavior modes to the Monte Carlo assessment's seven modes. From 2010-2020, the dark contour band traces the path of all simulations as the chloride front reached 50 mm and the concentration gradually increased. The wavy edges of the contours stem partially from the harmonic surface chloride concentration variation and partially from the damage measure discretization. At 2020, a small number of simulations were repaired with cathodic protection. The 2030 PDF's tightly banded distribution at 0.29 %wt/wt cement reflects variation in the mean annual temperature projection, including the noise term, as the apparent diffusion coefficient was a function of deterministic parameters and therefore incapable of contributing to

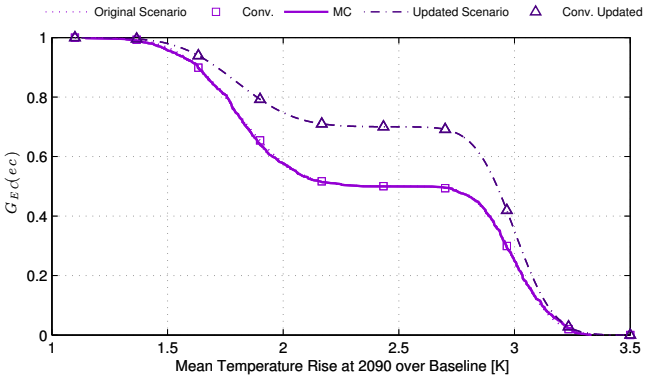

Figure 5: Characteristic exceedence distributions for increase in mean annual temperature from 1970 to 2090. Distributions are presented for the "original" distribution and both convolution discretization and Monte Carlo sampling, and for an "updated" higher-warming scenario with convolution discretization only.

the variance. Following the trend of highest density, a set of simulations continued on the same trajectory until end of service. These simulation's relatively high critical chloride concentrations prevented corrosion initiation. The 2030 PDF's large mass at zero chlorides revealed cathodic protection (CP) repair of some simulations at this time. Given that a CP system installed in 2030 would be expected to fail in 2060, with 20 years service remaining, it was inferred that these simulations were later repaired with cathodic protection (CPre). As shown in the vertical PDFs at 2050 and 2070, other simulation modes included later cathodic protection, up until the contours with repair at 2070 and 2080, which reflect either first application of patch repair, or patch repair after failure of the CP system. The trend of repair at 10-year intervals suggested that special inspections for corrosion triggered repair, rather than visual delamination inspection, which occurred at 2-year intervals. The small bandwidths of all contours indicated that the separation of the behavior into the different repair modes was due more to the stochastic corrosion initiation than variation in the characteristic exposure. The importance of the exposure scenario is discussed further in Sec. 5.3.

Corrosion rate distributions centered around relatively low rates ($< 0.1\mu A/cm^2$). The corrosion rates were on the lower end of the range for airborne chloride exposure in [4]. Due to the low corrosion rates and early repair times, reinforcement radius loss was negligible and delamination never occurred before 2080, which explained the lack of repairs following regular inspections.

5.1.3. Repair analysis results

Fig. 7 shows the probability mass function (PMF), p, for the convolution approach's eight and the Monte Carlo approach's seven active combinations. In

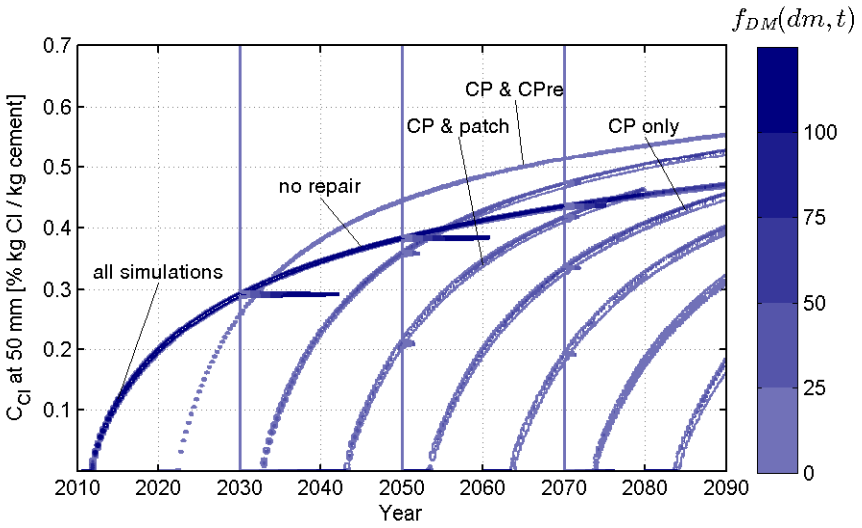

Figure 6: Evolution of probability density function for damage measure (DM) chloride concentration at 50 mm as a contour plot. Contours are plotted at $f_{DM} = \{1.5, 25, 50, 75, 100\}$. Probability density functions are plotted horizontally at $^1/_{20}$ scale against vertical axes at years 2030, 2050, and 2070.

both assessments the most common combination was no repair (combination 8). Several combinations consisting of only cathodic protection (combinations 4-6) and three multiple-repair combinations (1-3) also occurred. The Monte Carlo simulation resulted in fewer early repairs (combinations 1-2), and higher probability mass for combination 3. Investigation of the Latin hypercube and Monte Carlo samples indicated that several Latin hypercube critical chloride concentration samples were lower than the smallest Monte Carlo sample. These early-initiating simulations were responsible for the convolution approach's high probability masses at early repairs. Despite these discrepancies, the two-sample K-S test indicated a reasonable likelihood of distribution equivalency ($p = 0.39$).

5.1.4. Impact analysis results

Decision information results, shown in Fig. 8, were comprised of contributions from the eight active repair combinations. The central portion of the distributions differ between the two approaches, especially for cost (p=$\{0.56,0.76\}$ for $\{DI_1, DI_2\}$). The better agreement for downtime, which had only initial impact, suggested that the differences in repair timing probabilities for combinations 1-3 might have contributed to the different decision results. To determine whether the discrepancy was caused by the differences in repair timing combination probabilities or insufficient sampling of the decision variables, the Monte Carlo repair timing distribution was convolved with the convolution approach's conditional decision information distributions, yielding more robust

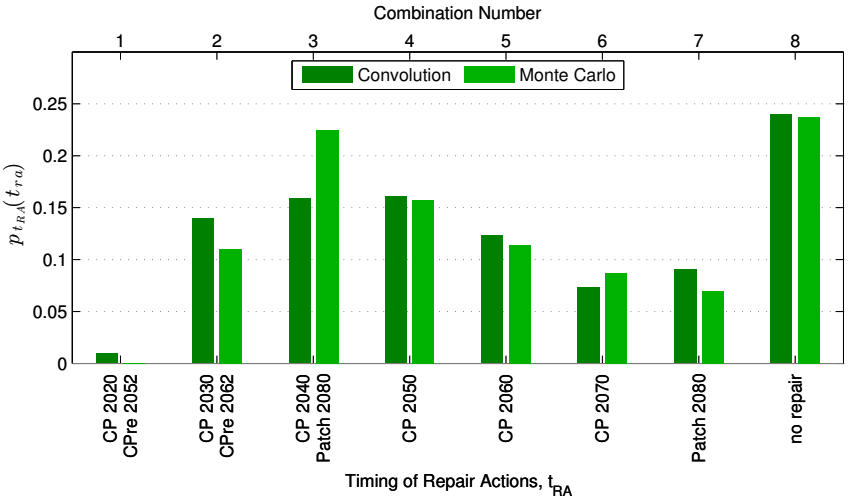

Figure 7: Probability mass function for combinations of repair action timing. Combination number is shown at the top of the figure.

Table 3: Decision information results for original convolution, original Monte Carlo, and convolution with updated exposure scenario.

Decision Information		Original, Convolution	Original, Monte Carlo	Updated Exposure, Convolution
Cost [USD]	$\mu_{di_1} \pm \sigma_{di_1}$	350 ± 217	354 ± 250	351 ± 195
	10% exceedence	682	656	682
Downtime [months]	$\mu_{di_2} \pm \sigma_{di_2}$	17.9 ± 9.8	18.5 ± 12.9	18.0 ± 9.6
	10% exceedence	33.2	33.1	33.2

final distributions. These distribution had better agreement with the convolution distribution (p=0.91 for both DI), which suggested that increasing the total number of Monte Carlo simulations would reduce the discrepancy. The remaining difference between the convolution and robust Monte Carlo approaches confirmed the role of the discrepant repair timing probabilities. Distribution moments and selected exceedence values are contained in Table 3. A statistical test of the distribution moments (Cohen's d) supported the finding of distribution equivalency (effect size 0.017).

5.2. Intermediate results

5.2.1. Conditional deterioration and repair analysis results

Conditional distributions for repair action timing combinations computed for the convolution approach are shown in Figure 9. Conditional damage measure results were similar to the fully convolved damage measure results for each discretized value of the characteristic exposure condition. The ten conditional repair timing PMFs were similar, with a slight trend towards late or no repair

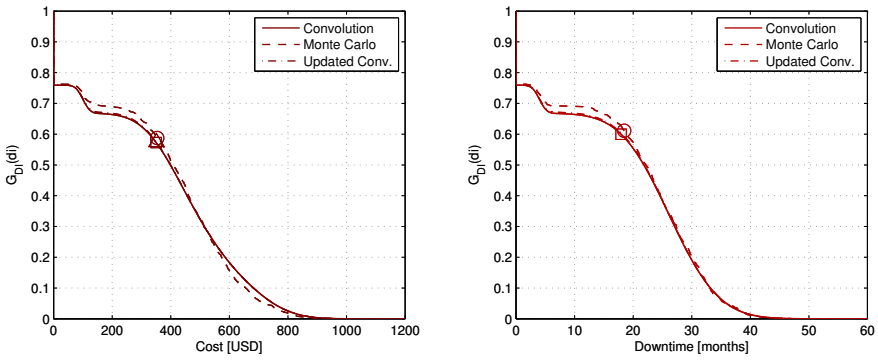

Figure 8: Exceedence distributions for lifetime decision information variables (a) cost and (b) downtime, for original and updated emissions scenarios. Means of the distribution are plotted as a square for the convolution approach, a circle for the Monte Carlo approach, and a triangle for updated convolution.

in the distributions with smallest increase in mean annual temperature. This behavior was consistent with the apparent diffusion model's prediction of faster chloride ingress at higher temperatures (see Appendix A).

5.2.2. Conditional impact analysis results

Impact analysis computed conditional distributions for cost and downtime for all possible combinations of repair action timing. Exceedence distributions for five of the eight active combinations are shown in Fig. 10. Besides the zero-impact "no repair" distributions, the lowest costs were incurred by combination 7, patch repair in 2080. The downtime distributions for combinations including only cathodic protection, as represented by combinations 3 and 4, were identical, as downtime was modeled as an initial, time-of-repair, impact. As expected, costs and downtimes were higher when multiple repairs took place, as occurred in combinations 6 and 7.

5.3. Deaggregation, backwards conditioning and updating of decision information

Whether convolution or Monte Carlo simulation is used to compute decision information distributions, the modularity of the PBDE framework facilitates studies to deaggregate uncertainty, trace uncertainty through backwards conditioning, and update results to reflect new data or models. Deaggregation is commonly used in probabilistic seismic hazard analysis to identify the contributions of various faults and events to the site seismic hazard. Deaggregation in PBDE can be used to assess how uncertainty in each of the three analysis stages contributes to the uncertainty in the final decision information results. Figure 11 presents deaggregation results in two ways. On the left, costs accrued over time are shown as 5%-95% probability envelopes for several combinations of deaggregated uncertainty. Starting from a deterministic result that assumes

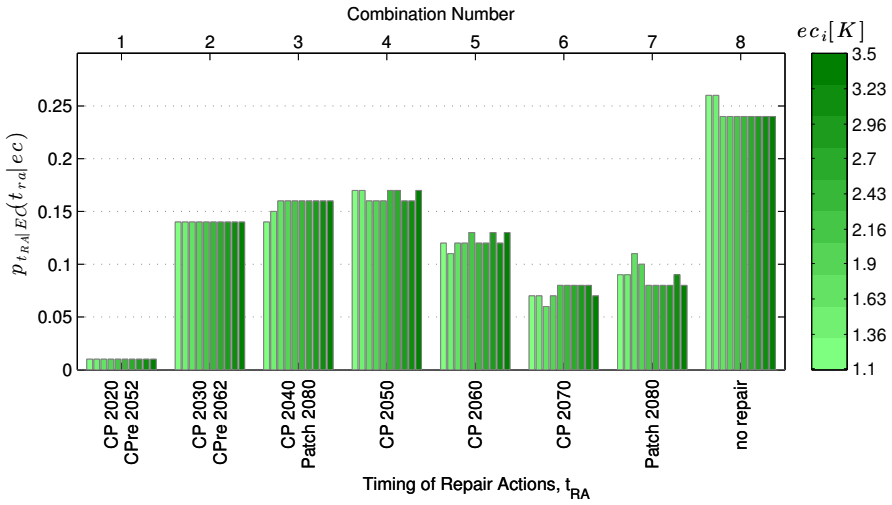

Figure 9: Conditional probability mass function for combinations of repair action timing, given a value of the exposure condition (ec) mean annual temperature rise at year 2090.

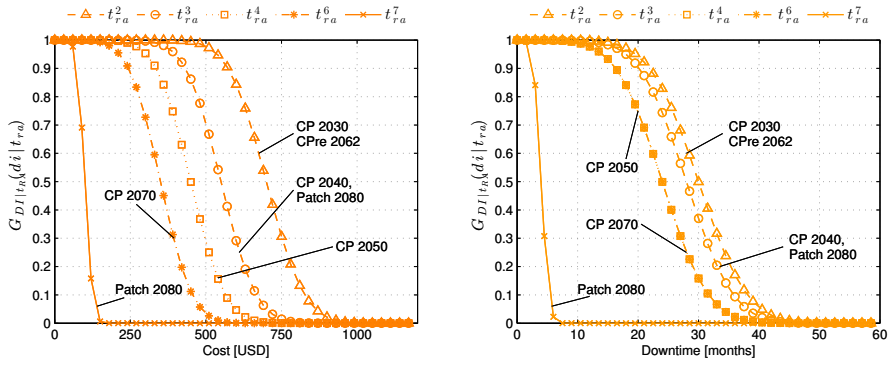

Figure 10: Conditional exceedence distributions for decision information variables (a) cost, and (b) downtime, for selected combinations (denoted in the legend with a superscript) of repair action timing.

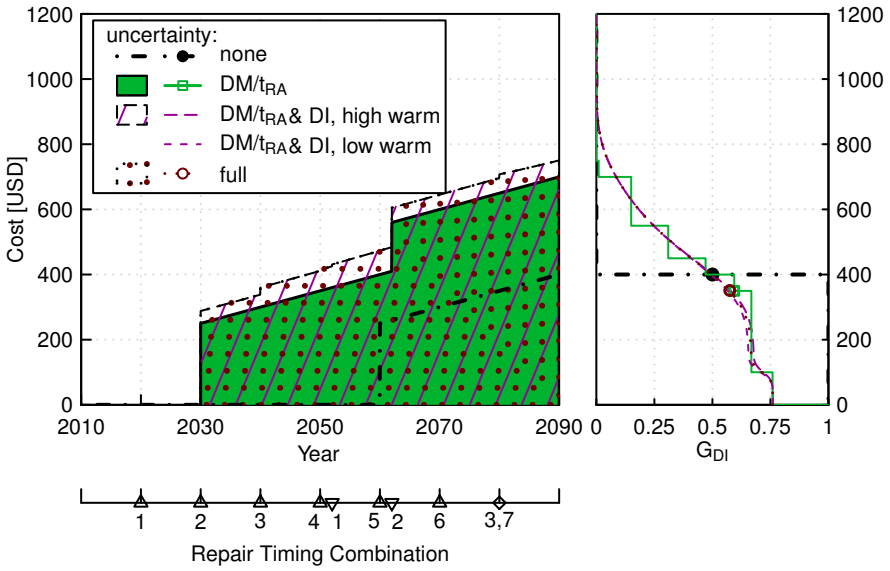

Figure 11: (a) Envelope for costs over time differentiated by types of uncertainty included. The dot-dashed line was obtained using expected values for exposure (results were identical for high and low warming scenarios), deterioration and repair parameters, and repair costs. The shaded area demarcated by the solid line includes uncertainty in damage and repair parameters (DM/t_{RA}). The hatched area demarcated by the long-dashed line includes additional uncertainty in repair costs (DI), for the expected exposure in the high warming scenario. The dotted area demarcated by the dotted line additionally considers the full distribution of exposure (i.e., the full PBDE assessment). (b) Complementary cumulative distribution functions for lifetime cost. Colors, markers and line styles are consistent with the legend in (a). Expected values for lifetime costs are plotted with a filled circle, square, and circle for no, DM/t_{RA}, and full uncertainty, respectively. Distributions obtained using the expected value for low as well as high warming are included. (c) Timeline for repair actions, including combination numbers. Upward-facing triangles denote cathodic protection; downward-facing triangles denote cathodic prevention; the diamond represents patch repair.

expected values for all parameters, the relative influence of analysis stage uncertainty can be determined by re-computing decision results while progressively including the uncertainty in each analysis stage. In the illustration, a large amount of cost uncertainty resulted from the inclusion of uncertainty in damage and repair analysis, and relatively less when uncertainty in impact analysis was additionally considered. Virtually no additional uncertainty resulted from including uncertainty in exposure analysis. On the right, the complementary cumulative distribution function also characterizes the relative importance of uncertainty in the three analysis stages. This plot identifies how the dispersion and expected value of cost changed as additional types of uncertainty were included. The PBDE framework's support for deaggregation through its modular structure is a major benefit of the approach.

For the example illustration, backwards conditioning was undertaken in or-

Figure 12: Conditional probability density function for decision information variable cost given an exposure condition value. The probability density function for the characteristic exposure conditions, original and updated, is shown at $^{1}/_{1000}$ scale.

der to obtain a more detailed characterization of the influence of the exposure condition, 80-year rise in mean annual temperature, on decision information. The results of backwards conditioning may be used to assess the effect of changing the characteristic exposure distribution to favor higher degrees of warming. As shown in Fig. 12, the decision information distributions were similar when conditioned on the range of exposure values. The irregularities in the surface reflect the variations in repair timing probabilities shown in Fig. 9. The similarity of the backwards-conditioned decision information distributions suggested that, for this illustration, a change in the exposure distribution would not greatly affect the decision information distributions, as was suggested by Fig. 11.

PBDE with convolution allows updating of one pinch-point distribution without requiring new analyses in other stages. An updated exposure distribution shown in Fig. 5 represented the hypothetical development of better climate models or evidence of high emissions. Updated decision information distributions were calculated by re-convolving conditional distributions with the updated exposure distribution, and are shown in Fig. 8. As expected, the updated scenario resulted in negligible changes to the cost and downtime distributions and decision metrics contained in Table 3.

6. Discussion

6.1. Illustration results and decision support

Results of the format shown in the example illustration could be used to better understand the likely deterioration of the structure and to improve the owner's inspection and repair scheme. The convolution approach predicted a 75% probability of corrosion initiation during the lifetime, which suggests that the concrete quality and cover depth were insufficient for the exposure. However, the inspection strategy led to repair before significant bar loss or delamination. Assessment of the repair results revealed that the most frequent contributors to the lifetime cost and downtime were repairs occurring during the first 30 years of service. The frequent multiple-repair scenarios were responsible for most of the probability of high costs and downtime. An owner wishing to reduce lifetime impacts might consider altering the repair strategy to delay repair, or use of a cathodic protection system that does not require removal of the concrete cover. Variation in the functional lifetime of the cathodic protection system was not considered, and would increase the uncertainty in cost and downtime associated with use of cathodic protection for periods greater than 20 years [47].

More generally, the decision information metrics computed by PBDE assessment allow improved selection of new designs or maintenance and repair schemes. In the illustration, while the expected value result accurately reflected the central tendency of the decision information distributions, it yields only one

decision metric. The computed decision information distributions allow use of numerous metrics, ranging from means or medians to critical exceedence values. A decision-maker might select an alternate design based on a lower cost value at 10% exceedence or a lower probability of exceeding some predetermined cost limit. These probabilistic decision metrics are expected to be more useful than a deterministic result, as they support risk-averse or risk-seeking strategies [31; 47]. While the computation of decision information distributions is not exclusive to PBDE, expected values for costs are more frequently used, e.g., in [13; 27; 28; 30; 47]. Additional decision support can be achieved through sensitivity assessment, for example by studying the impact of the damage measure thresholds on decision information. Multi-attribute decision optimization approaches, such as those discussed in Sec. 2.1.2 could be combined with sensitivity assessment to provide further decision support.

6.2. Comparison of convolution and Monte Carlo approaches

The main study indicated that the convolution and Monte Carlo approaches yielded statistically equivalent results at the same number of damage/repair simulations. Certain techniques, e.g., fitting parametric distributions for repair and deterioration conditional distributions, could potentially reduce the required number of convolution simulations. Combination of Monte Carlo exposure/deterioration/repair simulation with analytical computation of decision information distributions may have allowed reduction of the number of Monte Carlo simulations.

While both the convolution and Monte Carlo approaches are modular, the convolution approach offers some advantages. Assessment of the role of exposure on deterioration, repair, and impact was made through easily accessible intermediate convolution results, but would require additional analysis for the Monte Carlo approach. Similarly, deaggregation and backwards conditioning results were obtained by manipulating the convolution integral but are difficult to obtain with high robustness using Monte Carlo. Updating of results based on changes to exposure was simply computed using convolution, but would require bootstrapping or additional simulation for the Monte Carlo approach. The deaggregation illustration indicated negligible influence of the exposure condition on decision information, which made updating and re-convolution superfluous. However, the lack of sensitivity to mean annual temperature increase suggests the possibility of secondary conditioning on the mean annual temperature noise term to determine if that term had a larger effect on the decision information results. Such secondary conditioning can be easily incorporated into the convolution integral in Eq. 1 through the addition of a secondary exposure conditional distribution.

6.3. Sensitivity of damage and decision information to climate change

While sensitivity of chloride ingress and corrosion to climate change in this illustration was similar to that seen in other studies, e.g., [3; 6], decision outcomes may differ. These studies found up to a 15% earlier onset of damage or

reduced service life when climate change from approximately 2000 to 2100 is considered. Bastidas-Arteaga et. al [6] finds larger variance in sensitivity, from 1.7 to 31% reduction in mean time to failure determined through structural reliability analysis, depending on the severity of climate change, the exposure, and the corrosiveness of the local environment. Results from this study agree that corrosion initiation and cracking times may be reduced when climate change is considered. However, the extension to repair and impact analysis herein suggests that a reduction in apparent service life does not necessarily result in an increase in impacts due to the mitigating effect of current and presumed future repair strategies. Stewart and Peng [5] performed life cycle costing of various adaptation measures and found that while increasing concrete cover depth slows the onset of deterioration, it is not a rational strategy from a life-cycle costing perspective. All studies advise that their results do not provide conclusive prediction of the impact of climate change on corrosion in reinforced concrete. More work is needed to assess how accelerated deterioration, repair, and impacts interact before general conclusions can be drawn on appropriate climate adaptation strategies.

In this example, uncertainty in repair timing and the variances of conditional decision information distributions had a more significant influence than climate change severity on the final impact distributions. For the illustration example, more research and modeling effort should be directed towards decreasing epistemic uncertainty in conditional decision information models, as the uncertainty in repair timing is thought to reflect natural variability in structural deterioration. Inclusion of spatial variation of deterioration parameters, rather than consideration of deterioration parameter uncertainty over multiple simulations, might allow for a reduction of the number of required simulations. Use of more sophisticated deterioration models would be expected to increase the uncertainty in damage and repair if the sophistication of exposure models was also suitably increased, as suggested in [6].

6.4. Modeling extensions for the illustration example

In each analysis stage the models selected aimed for a reasonable degree of accuracy and low computational expense; use of different models or assumptions may have significantly changed the results. Certain assumptions facilitated accuracy in the analysis, including the vertical orientation of the sheltered surface, location of the site in a tropical region, and selection of a single deterioration mechanism. Other assumptions, such as the use of ambient meteorological data as exposure conditions, and the use of generic decision information, may have decreased the potential for accuracy. Important areas for future sensitivity analysis achievable within the convolution approach follow.

The exposure analysis approach ignored many nonlinearities, including possible increases in local weather variability caused by global climate change. However, the deterioration models used were insensitive to fluctuations in temperature and relative humidity at short time scales, which decreased the effect of omitting the complex nonlinearities. The assumption of constant relative humidity and chloride exposure with increasing mean annual temperature has been

widely used, but is controversial, especially considering regional scale climate changes [49]. Use of a more sophisticated heat, moisture, and ion transport model would enable the assessment of the impact of the assumptions of stationary variability, relative humidity, and chloride exposure on decision information.

Multi-physics models for corrosion in reinforced concrete have been developed, e.g., [35; 50–52], which should be capable of assessing sensitivity to climate parameters. These models also close the deterioration analysis loop by linking cracking to boundary conditions and transport, which render them more effective for lengthy inspection intervals. On the other hand, empirical models, such as the dose-response models and factor methods [53] used for assessment of building envelopes, are computationally efficient, which allows for greater consideration of uncertainty, e.g., in material properties. Both multi-physics and empirical approaches can be improved by consideration of spatial variation of damage. Accounting for partial spatial correlation would require the use of two- or three-dimensional models, additional damage/repair simulations, bootstrapping, or correlation functions to simulate the states of multiple structural areas. Techniques for reducing computational expense, such as those discussed in Section 3.6, are likely necessary for implementation of advanced models and partial spatial correlation in PBDE assessment.

Assumptions made in repair analysis complemented the level of sophistication of deterioration modeling, but could be made more realistic. Repairs were assumed to occur immediately following inspection. Use of stochastic delay of a repair following an investigation, or stochastic damage measure thresholds to mimic imperfect inspection techniques, would be straightforward to implement and would increase realism. More significantly, the necessity of maintaining safety and the prevalence of life-cycle costing suggest considering predictions of future deterioration and cost when selecting an appropriate repair. Safety risks were unlikely in this example, but a more sophisticated analysis would need to include a structural analysis and reliability model.

Finally, impact analysis could be improved through the use of more sophisticated cost, downtime, and environmental impact modeling, e.g., process-based approaches [37; 38]. These approaches would mitigate the error associated with indirect applicability of repairs made to different structures, inflation, and local variations in prices and practices, but take substantial effort to implement. More readily made improvements would include consideration of cost and downtime for the inspections themselves, study of the impact of correlated decision information variables, and use of net-present-value calculations.

6.5. Future work

In addition to the modeling extensions discussed in Section 6.4, research is required to further develop the PBDE framework in several areas. Notably, work is needed to demonstrate the incorporation of multiple deterioration mechanisms, and to implement techniques to increase computational efficiency. These efforts would prove useful in an attempt to validate the framework on a case study structure. Successful validation on a case study structure would demonstrate the viability of the models used in the analysis stages and the framework

more generally. Sensitivity assessment or updating using the case study results could demonstrate the value of the convolution approach.

The convolution approach's advantages of deaggregation, backwards conditioning and updating would likely hold for other analyses with no coupling between analysis stages (i.e., valid conditional independence) and assessments where the assumption of de-coupling is reasonable. For example, assessments of bridge scour, building façade damage, or deterioration of steel infrastructure allow the same general assumptions of conditional independence. While the assessment of an infrastructure network where repair decisions are made based on the status of a number of structures would be computationally challenging, such an assessment would meet the requirements of the convolution approach.

Some assessments may violate the assumption of conditional independence between analysis stages. If, for example, a study assumes that the cost of future energy depends on the severity of climate change, exposure and impact analysis would no longer be independent. In such a case, it may be acceptable to assume conditional independence and make consistent assumptions in computing exposure condition and conditional decision-information distributions. Alternately, Monte Carlo simulation may be used to ensure accuracy. If the Monte Carlo approach is used, it is still possible to perform updating or sensitivity assessment, although these tasks become more difficult. Strict requirement of conditional independence hinders the implementation of PBDE in "integrated assessments," which are becoming more common in climate change impact studies. While integrated assessments allow study of the interaction of policy, climate, and infrastructure performance, they require feedback loops between analysis stages, thereby reducing the conceptual clarity offered by the PBDE framework.

Suggested applications of the PBDE framework include studies of archetype structures for use in design code calibration, climate change adaptation policy studies, and sensitivity studies to direct future research. Previous efforts have utilized performance-based approaches to "rationalize" seismic rehabilitation provisions [20]; similar efforts could be undertaken using the PBDE framework. Planning for climate change adaptation requires a multi-attribute decision framework, and must contend with the high level of uncertainty associated with future emissions, climate response, and climate change impacts. The PBDE framework can accommodate these desirable features, and PBDE's computational expense may be acceptable for major regional studies. Finally, the modularity of the PBDE framework supports testbed comparison of models used in the analysis stages, e.g., deterioration analysis, for which there are many available models and limited data on the decision implications of model selection. Due to the high computational expense of PBDE, other methods, such as Markov chains or artificial intelligence techniques, may be preferred for network-level optimization. Similarly, routine decision-making for multi-mechanism deterioration of common structure types may be better supported by service-life prediction methods.

7. Conclusions

A modular framework for performance-based durability engineering (PBDE) assessment has been proposed. The methodology is similar to those of frameworks developed for a variety of engineering risk assessments, and uses models developed for service life and durability assessment. By linking uncertainty in analysis of exposure, deterioration and repair, and impacts, this methodology can assess the economic, environmental, and social sustainability of structures in a fully probabilistic manner. Additionally, by comprehensively modeling from exposure to impacts, the framework is sufficiently general to assess new structure types and materials, and is accommodating of shifts in weather patterns caused by climate change. When applicable, the proposed convolution-based methodology for PBDE offers improvement over traditional Monte Carlo simulation in implementing deaggregation and backwards conditioning, which allow identification of important sources of uncertainty. Additionally, PBDE's modularity facilitates updating of results to reflect new data or models.

Future work to address the interaction of deterioration mechanisms and the computational expense associated with the methodology is needed to support the application of PBDE in three targeted domains. PBDE's consideration of uncertainty from exposure to impacts may aid design code calibration, especially when considering the potential effects of climate change on structural durability. The PBDE framework's prediction of probabilistic distributions for economic, social, and environmental sustainability metrics is thought advantageous in guiding policy, e.g., climate change adaptation planning. Finally, flexibility in choice of models allows researchers to assess the effects of model and parameter selection to direct future work. The proposed PBDE framework has a clear, modular structure, efficiently combines multiple sources of uncertainty, and supports analysis of the influence of various uncertainty sources on decision results.

Acknowledgements

The authors thank Mette Geiker and Alexander Michel for their assistance with deterioration modeling and developing reasonable deterioration and repair assumptions. Jan-Magnus Østvik, Claus Larsen, Arne Gussiås, Ragnhild Relling, and Knut Grefstad are acknowledged for their help in selecting repair strategies and developing estimates of repair impacts. Hans Janssen is thanked for sharing his Latin hypercube optimization routine. Additionally, this work was made possible by the following funding: the National Science Foundation Graduate Research Fellowship Program and Nordic Research Opportunity, the Stanford Gabilan Graduate Fellowship, the John A. Blume Earthquake Engineering Center at Stanford University, and the UPS Foundation at Stanford University.

Appendix A. Deterioration models

The chloride ingress model used is a nonlinear apparent diffusion model similar to the apparent diffusion model in [24], and to the ion diffusion equation in [6]. The nonlinear influence of chloride binding on diffusion was modeled as in [36], requiring use of numerical methods to solve the partial differential equation [45]. Whereas [36] solves coupled partial differential equations for heat and mass transport, this study neglected ion transport caused by migration and convection and assumed instantaneous heat and moisture equilibrium with surface conditions. This results in a partial differential equation governing apparent chloride diffusion, Eq. A.1, where C_{Cl} is the chloride concentration and D_{Cl} the apparent diffusion coefficient. As reported in [36] the assumption of instantaneous heat and moisture equilibrium is not generally valid and may lead to errors in prediction of chloride ingress. However, chloride ingress models that accept non-stationary boundary conditions are scarce, and fully-coupled heat and mass transport models were prohibitively computationally expensive for a dual convolution/Monte Carlo assessment. Thus the dependence of the chloride diffusion coefficient on concrete absolute temperature T, relative humidity h, chloride content, and aging was maintained as shown in Eq. A.2. The reference apparent diffusion coefficient, D^0_{Cl}, was taken from [24] for ordinary portland cement concrete with water to cement ratio of 0.5. The temperature dependence took the form of an Arrhenius rate law, Eq. A.3, where the activation energy, U, was taken from [24]. Moisture-dependency was modeled according to Eq. A.4, also used in [6]. The effect of chloride binding on the diffusion coefficient was modeled using a Langmuir binding isotherm, Eq. A.5 [36], where C_{Cl} is expressed in moles per cubic meter, assuming 350 kg cement content. Aging was accounted for using Eq. A.6 from [24]. Parameters for chloride ingress and all other required material parameters are given in Table A.4.

$$\frac{\partial C_{Cl}}{\partial t} = \nabla \left(D_{Cl} \nabla C_{Cl} \right) \tag{A.1}$$

$$D_{Cl}(T, h, C_{Cl}) = D^0_{Cl} f_T(T) f_h(h) f_{bind}(C_{Cl}, \theta_l) f_{age}(t) \tag{A.2}$$

$$f_T(T) = \exp\left(\frac{U}{R} \left(\frac{1}{T_{\text{ref}}} - \frac{1}{T} \right) \right) \tag{A.3}$$

$$f_h(h) = \left(1 + \frac{(1-h)^4}{(1-h_c)^4} \right)^{-1} \tag{A.4}$$

$$f_{\text{bind}}(C_{Cl}, \theta_l) = \frac{1}{1 + \alpha_{\text{bind}} / \left(\theta_l (1 + \beta_{\text{bind}} C_{Cl})^2 \right)} \tag{A.5}$$

$$f_{age} = \max\left(\left({}^{t_0}/_{t} \right)^m, 0.1 \right) \tag{A.6}$$

Some of these equations require translating concrete relative humidity first to capillary pressure, p_c, according to Eq. A.7, where ρ_l is the mass density of liquid water, R the gas constant, and M_l the molar mass of water. Capillary pressure was converted to moisture content by volume, θ_l, according to a moisture storage

function of the van Genuchten type, Eq. A.8. θ_{cap} is the maximum capillary moisture content, a_i, n_i and m_i are shape parameters and l_i a weighting factor. The moisture content can be expressed relative to concrete mass, w, through Eq. A.9.

$$p_c = \frac{-\rho_l RT}{M_l} \ln h \tag{A.7}$$

$$\theta_l = \theta_{\text{cap}} \sum_{i=1}^{k} \frac{l_i}{\left(1 + (a_i p_c)^{n_i}\right)^{m_i}} \tag{A.8}$$

$$w = \theta_l \frac{1/\rho_l}{1/\rho_{\text{conc}}} \tag{A.9}$$

The partial differential equation (Eq. A.1) was solved in one dimension using a 1 mm uniform mesh from 0-65mm, 5mm mesh from 70-80 mm, and 10mm mesh from 90-250mm depth. The initial condition was no chloride content, the external boundary condition was a Dirichlet boundary of the surface chloride concentration function, and the inner boundary condition was a Neumann "no flux" condition. The transport output time step was 0.04 years. Internal transport time steps were chosen by the solver.

Corrosion modeling took place at each transport output time step. Reinforcement corrosion initiation was tested against a stochastic value of the critical chloride content, C_{Cl}^{cr}, which was modeled as lognormally distributed with mean and standard deviation in the range used in [3; 6; 24]. Assumption of a constant critical chloride content for each simulation is a simplification of a complex phenomena, but matched the level of sophistication of the other deterioration models [54]. Reinforcement corrosion current density, i_{corr} [μA/cm^2], was calculated using a commonly-used empirical model from Liu and Weyers [55] which considers the effect of chloride concentration at rebar depth [kg/m^3], temperature [K], concrete resistance, R_c [Ω], and time since corrosion initiation, t_c [yr]. It also includes an aleatoric component, leading to a lognormally distributed random variable for i_{corr}. The corrosion rate model assumes sufficient oxygen availability for the anodic reaction, which is reasonable given the assumed concrete relative humidity and moisture content [42; 56; 57]. Concrete resistance was assumed constant at 25 kΩ, which reflected a moderate degree of capillary saturation [57]. Concrete resistivity changes by orders of magnitude depending on the moisture content, which would suggest the use of a moisture-dependent resistance value, but Eq. A.10 likely considers moisture content indirectly through the chloride and temperature dependence, and this effect was omitted.

$$\ln 1.08 i_{\text{corr}} = 7.89 + 0.7771 \ln\left(1.69 C_{Cl}\right) - 3006/T - 0.000116 R_c + 2.24 t_c^{-0.215} + N\left(0, 0.3312\right) \tag{A.10}$$

Reinforcement cross section reduction was calculated from Faraday's law, Eq. A.11. Here M_{Fe} is the molar mass of iron, z_{Fe} is the charge number for iron in

the corrosion reaction, F is Faraday's constant, and ρ_{steel} is the density of steel. z_{Fe} of 2 was assumed based on the thermodynamic considerations presented in [56] and reflecting the formation of Fe_2O_3 at the anodic site. Numerical integration assumed constant i_{corr} over the time intervals.

$$\Delta r = \int \frac{i_{\text{corr}} M_{\text{Fe}}}{z_{\text{Fe}} F \rho_{\text{steel}}} \, \mathrm{d}t \tag{A.11}$$

Due to the computational expense associated with sophisticated methods of predicting delamination or cracking, a simplified approach was used. Coastal exposure can lead to the formation of aqueous rust products that may diffuse away from the reinforcement without causing a buildup of pressure, further complicating the prediction of cracking. In this analysis it was assumed that the rust product formed was Fe_2O_3, hematite, which is not aqueous, and has a volume ratio to iron of approximately 2.1 [56]. Based on empirical results for ordinary Portland cement concretes of similar assumed w/c ratio, bar radius loss to produce delamination or cover cracking was modeled as lognormally distributed with mean of 40 µm and standard deviation of 10 µm [58]. As with assumptions regarding corrosion initiation and rate, the use of a stochastic delamination prediction greatly simplifies the complex kinetics and mechanics of crack formation, but was selected as a reasonable assumption for illustration of the PBDE methodology.

References

[1] ASCE, 2013 ASCE Report Card for America's Infrastructure, 2013.

[2] US FHWA, National Bridge Inventory, US FHWA, 2013.

[3] X. Wang, M. G. Stewart, M. N. Nguyen, Impact of climate change on corrosion and damage to concrete infrastructure in Australia, Clim Chang 110 (2012) 941–957.

[4] M. G. Stewart, X. Wang, M. N. Nguyen, Climate change impact and risks of concrete infrastructure deterioration, Eng Struct 33 (2011) 1326–1337.

[5] M. G. Stewart, J. Peng, Life cycle cost assessment of climate change adaptation measures to minimise carbonation-induced corrosion risks, Int J Eng Uncertain: Haz Assess Mitig 2 (2010) 35–46.

[6] E. Bastidas-Arteaga, F. Schoefs, M. G. Stewart, X. Wang, Influence of global warming on durability of corroding RC structures: A probabilistic approach, Eng Struct 51 (2013) 259–266.

[7] F. Rendell, R. Jauberthie, M. Grantham, Deteriorated Concrete: Inspection and Physiochemical Analysis, Thomas Telford, London, 2002.

[8] O. C. C. D. US EPA, Inventory of U.S. Greenhouse Gas Emissions and Sinks, Technical Report EPA 430-R-13-001, US EPA, Washington, DC, 2013.

Table A.4: Parameters for heat and mass transport, corrosion, and delamination models

	Model Parameter	Symbol	Value	Unit	Source
Initial	initial relative humidity	h_{init}	0.74	[-]	-
conditions	initial absolute temperature	T_{init}	295	[K]	-
Chloride	chloride diffusion coefficient	D_{Cl}^{0}	15.8E-12	[m^2/s]	[24]
transport	repair chloride diffusion coefficient	D_{Cl}^{0}	30.0E-12	[m^2/s]	[6]
parameters	activation energy for chloride diffusion	U	40	[kJ/mol]	[24]
	gas constant	R	8.314E-03	[kJ/mol]	-
	reference temperature	T_{ref}	293	[K]	[24]
	moisture correction factor	h_c	0.75	[-]	[6]
	aging coefficient	m	3	-	[24]
	reference time	t_0	28	[days]	[24]
	non-physical binding parameter	α_{bind}	4	-	[36]
	non-physical binding parameter	β_{bind}	3.3	-	[36]
Moisture	non-physical parameter	l_1	0.462	-	[36]
storage	non-physical parameter	l_2	0.574	-	[36]
parameters	non-physical parameter	n_1	2.34	-	[36]
	non-physical parameter	n_2	2.68	-	[36]
	non-physical parameter	a_1	2.4E-08	-	[36]
	non-physical parameter	a_2	2.5E-07	-	[36]
	non-physical parameter	m_1	$1-1/n_1$	-	[36]
	non-physical parameter	m_2	$1-1/n_2$	-	[36]
	max. capillary moisture content	θ_{cap}	0.116	[m^3/m^3]	[36]
	molar mass of water	M_l	0.018	[kg/mol]	-
	mass density of water	ρ_l	1000	[kg/m^3]	-
	mass density of concrete	ρ_{conc}	2400	[kg/m^3]	-
Corrosion	mean critical chloride content	$\mu_{c_{Cl}^{\mathrm{cr}}}$	0.40	[%wt cem]	[3; 6; 24]
initiation &	std. dev. of critical chloride content	$\sigma_{c_{Cl}^{\mathrm{cr}}}$	0.10	[%wt cem]	[3; 6; 24]
propagation	concrete cover resistance	R_c	25	[kΩ]	[57]
Reinforcement	charge number for iron	z_{Fe}	2	[e]	[56]
radius	Faraday's constant	F	96500	[C/mol]	-
reduction	molar mass of iron	M_{Fe}	55.85	[g/mol]	-
	density of steel	ρ_{steel}	7850	[kg/m^3]	-
Delamination	mean critical radius reduction	$\mu_{\Delta r^{\mathrm{cr}}}$	40	[µm]	[58]
	std. dev. critical radius reduction	$\sigma_{\Delta r^{\mathrm{cr}}}$	10	[µm]	[58]

[9] WBCSD, Cement Technology Roadmap 2009, Technical Report, OECD/IEA, World Business Council for Sustainable Development, 2009.

[10] US GAO, Highway Bridge Program: Clearer Goals and Performance Measures Needed for a More Focused and Sustainable Program, Technical Report GAO 08-1043, US-GAO, 2008.

[11] fib, Model Code, First complete draft, fib, 2010.

[12] P. Bocchini, D. Saydam, D. M. Frangopol, Efficient, accurate, and simple Markov chain model for the life-cycle analysis of bridge groups, Struct Saf 40 (2013) 51–64.

[13] J. Qin, M. H. Faber, Risk Management of Large RC Structures within Spatial Information System, Comput-Aided Civ Infrastruct Eng 27 (2012) 385–405.

[14] F. Altmann, V. Mechtcherine, Durability design strategies for new cementitious materials, Cem Concr Res 54 (2013) 114–125.

[15] O. E. Gjørv, Durability design of concrete structures in severe environments, Durability design of concrete structures in severe environments, Taylor & Francis, New York, 2009.

[16] A. Azizinamini, H. C. Ozyildirim, E. H. Power, E. S. Kline, Design Guide for Bridges for Service Life, Technical Report R19A, TRB, SHRP 2, 2013.

[17] DuraCrete, General Guidelines for Durability Design and Redesign, Technical Report 15, EU Brite EuRam III, 2000.

[18] S. Kaplan, B. J. Garrick, On the quantitative definition of risk, Risk Analysis 1 (1981) 11–27.

[19] G. G. Deierlein, H. Krawinkler, C. A. Cornell, A framework for performance-based earthquake engineering, in: Pac Conf Earthq Eng, pp. 1–8.

[20] R. O. Hamburger, The ATC 58 Project: Development of next generation performance based earthquake engineering design criteria for buildings, in: Struct Congr, ASCE, 2006, pp. 1–8.

[21] M. Flint, S. L. Billington, Implementation of multiscale models in a probabilistic framework for performance-based durability engineering, in: R. Borja (Ed.), Int Workshop Multiscale Multiphys Process Geomech, Springer, Stanford, USA, 2010, pp. 1–4.

[22] A. A. Sohanghpurwala, Manual on Service Life of Corrosion-Damaged Reinforced Concrete Bridge Superstructure Elements, Technical Report 558, NCHRP, 2006.

[23] D. V. Val, R. E. Melchers, Reliability of deteriorating RC slab bridges, J Struct Eng (1997) 1638–1644.

[24] fib, Bulletin 34: Model Code for Service Life Design, Technical Report, fib, Lausanne, 2006.

[25] R. Rackwitz, A. Joanni, Risk acceptance and maintenance optimization of aging civil engineering infrastructures, Struct Saf 31 (2009) 251–259.

[26] F. Biondini, F. Bontempi, D. M. Frangopol, P. G. Malerba, Cellular automata approach to durability analysis of concrete structures in aggressive environments, J Struct Eng 130 (2004) 1724–1737.

[27] V. Patidar, S. Labi, K. C. Sinha, P. D. Thompson, Multi-objective optimization for bridge management systems, Technical Report 590, NCHRP, 2007.

[28] E. Bastidas-Arteaga, F. Schoefs, Stochastic improvement of inspection and maintenance of corroding reinforced concrete structures placed in unsaturated environments, Eng Struct 41 (2012) 50–62.

[29] M. Ciampoli, F. Petrini, G. Augusti, Performance-Based Wind Engineering: towards a general procedure, Struct Saf 33 (2011) 367–378.

[30] J. E. Padgett, C. Tapia, Sustainability of Natural Hazard Risk Mitigation: A Life-Cycle Analysis of Environmental Indicators for Bridge Infrastructure, J Infrastruct Syst 19 (2013) 130723224919000.

[31] M. E. Paté-Cornell, Uncertainties in risk analysis: Six levels of treatment, Reliab Eng Syst Safe 54 (1996) 95–111.

[32] N. Nakicenovic, J. Alcamo, G. Davis, B. de Vries, Special report on emissions scenarios: a special report of Working Group III of the Intergovernmental Panel on Climate Change, Technical Report, IPCC, 2000.

[33] N. Luco, C. A. Cornell, Structure-Specific Scalar Intensity Measures for Near-Source and Ordinary Earthquake Ground Motions, Earthq Spectra 23 (2007) 357–392.

[34] H. Janssen, B. Blocken, J. Carmeliet, Conservative modelling of the moisture and heat transfer in building components under atmospheric excitation, Int J Heat Mass Transf 50 (2007) 1128–1140.

[35] A. Michel, M. R. Geiker, H. Stang, M. D. Lepech, Integrated modelling of corrosion-induced deterioration in reinforced concrete structures, in: EuroCorr, Estoril, Portugal, pp. 1–5.

[36] M. Flint, A. Michel, S. L. Billington, M. R. Geiker, Influence of temporal resolution and processing of exposure data on modeling of chloride ingress and reinforcement corrosion in concrete, Mater Struct (2013) 1–20.

[37] R. Kirchain, Cost modeling of materials and manufacturing processes, in: Encyclopedia of Materials: Science and Technology, Elsevier B.V., 2001, pp. 1–10.

[38] D. Cass, A. Mukherjee, Calculation of greenhouse gas emissions for highway construction operations by using a hybrid life-cycle assessment approach , J Constr Eng Manag 137 (2011) 1015–1025.

[39] J. Hammervold, M. Reenaas, H. Brattebø, Environmental Life Cycle Assessment of Bridges, J Bridge Eng 18 (2013) 153–161.

[40] K. A. T. Vu, M. G. Stewart, Predicting the likelihood and extent of reinforced concrete corrosion-induced cracking, J Struct Eng 131 (2005) 1681–1689.

[41] A. J. O'Connor, O. Kenshel, Experimental evaluation of the scale of fluctuation for spatial variability modeling of chloride-induced reinforced concrete corrosion, J Bridge Eng 18 (2013) 3–14.

[42] K. G. Papakonstantinou, M. Shinozuka, Probabilistic model for steel corrosion in reinforced concrete structures of large dimensions considering crack effects, Eng Struct 57 (2013) 306–326.

[43] H. Janssen, Monte-Carlo based uncertainty analysis Sampling efficiency and sampling convergence, Reliab Eng Syst Safe 109 (2013) 123–132.

[44] T. R. Karl, J. M. Melillo, T. C. Peterson, Global climate change impacts in the United States, Technical Report, US Global Change Research Program, 2009.

[45] T. Luping, J. Gulikers, On the mathematics of time-dependent apparent chloride diffusion coefficient in concrete, Cem Concr Res 37 (2007) 589–595.

[46] B. G. M. Husslage, G. Rennen, E. R. Dam, D. Hertog, Space-filling Latin hypercube designs for computer experiments, Optim Eng 12 (2010) 611–630.

[47] R. B. Polder, G. Leegwater, D. Worm, W. Courage, Service life and life cycle cost modelling of cathodic protection systems for concrete structures, Cem Concr Compos (2013) 1–6.

[48] C. Nerland, J. Eri, K. A. Grefstad, Ø. Vennesland, 18 years of Cathodic Protection of Reinforced Concrete Structures in Norway – facts and figures from 162 installations, in: Eurocorr07, Freiburg, pp. 1–8.

[49] K. M. Willett, Creation and analysis of HadCRUH, Ph.D. thesis, University of East Anglia, Norwich, 2007.

[50] K. Maekawa, T. Ishida, T. Kishi, Multi-scale modeling of structural concrete, Taylor & Francis Group, New York, 2009.

[51] T. Pan, L. Wang, Finite-element analysis of chemical transport and reinforcement corrosion-induced cracking in variably saturated heterogeneous concrete, J Eng Mech 137 (2011) 334–345.

[52] J. Ožbolt, G. Balabanić, M. Kušter, 3D Numerical modelling of steel corrosion in concrete structures, Corrosion Science 53 (2011) 4166–4177.

[53] P. J. Hovde, K. Moser, Performance based methods for service life prediction, Technical Report 294, CIBW080, 2004.

[54] U. Angst, B. Elsener, C. K. Larsen, Vennesland, Critical chloride content in reinforced concrete, Cem Concr Res 39 (2009) 1122–1138.

[55] T. Liu, R. W. Weyers, Modeling the dynamic corrosion process in chloride contaminated concrete structures, Cem Concr Res 28 (1998) 365–379.

[56] A. Küter, Management of Reinforcement Corrosion: A Thermodynamic Approach, Ph.D. thesis, DTU Department of Civil Engineering, Kongens Lyngby, Denmark, 2009.

[57] E. J. Sellevold, Resistivity and humidity measurements of repaired and non-repaired areas in Gimsøystraumen Bridge, in: A. Blankvoll (Ed.), Int Conf Repair Concr Struct, NPRA, Svolvær, Norway, pp. 283–295.

[58] A. O. S. Solgaard, A. Michel, M. R. Geiker, H. Stang, Concrete cover cracking due to uniform reinforcement corrosion, Mater Struct 46 (2013) 1781–1799.